ARTICLES

Red Edge Photophysics of Ethanolic Rhodamine 101 and the Observation of Laser Cooling in the Condensed Phase

J. L. Clark, P. F. Miller, and G. Rumbles*

Department of Chemistry and Centre for Photomolecular Science, Imperial College of Science, Technology and Medicine, London, SW7 2AY, United Kingdom

Received: December 22, 1997

Laser cooling in fluid solutions of the laser dye rhodamine 101 in acidified ethanol has been observed when the molecule is excited into the low-energy tail of the absorption spectrum, at energies in the region 585−1593 cm^{-1} lower in energy than the 0−0 band origin at 590 nm. The most efficient cooling is achieved when the laser is tuned to 615 nm when a net cooling power of 0.37 mW per 100 mW of pumping power is observed. In this paper, details leading up to this unique observation are documented: in particular, the quantum efficiencies in highly concentrated solutions and the characterization of anti-Stokes fluorescence as a nonintrusive temperature sensor.

Introduction

In 1946 Pringsheim[1] and Vavilov[2] pointed out the possibility of optical cooling for fluorescent solids when excited in the long wavelength region of the absorption spectrum. The thermodynamics of this theory was developed by Landau.[3] Experimentally, such cooling by anti-Stokes fluorescence was first observed in the gaseous phase when a 1 °C drop in temperature was documented in carbon dioxide gas at 300 °C, when pumped with 10.6 μm light of a carbon dioxide laser.[4] Previous to this, several attempts had been made to observe the effect in solids. These included cooling by the irradiation of Cr^{3+} ions in ruby[5] and the cooling of Nd^{3+}-doped yttrium aluminium garnet[6] crystals. However, both these attempts displayed only a reduced amount of sample heating. More recently a direct observation of this theory has been demonstrated by Epstein et al.,[7,8] who reported the laser-induced fluorescent cooling of a heavy-metal-fluoride glass (ZBLANP) doped with trivalent ytterbium ions. They report a reduction of 16 K from room temperature when the sample is incorporated into an optical fiber.

Laser cooling has also been attempted in liquid solutions of xanthene laser dyes. Zander and Drexhage[9] inferred changes in a thermal lens signal when a 3.5×10^{-6} M solution of rhodamine 6G in deuterated ethanol was irradiated in the long wavelength region as being due to a small, but immeasurable, temperature decrease. Later we made the first direct observation of photoluminescence laser cooling in a solution phase using an organic dye molecule as the active moeity:[10] A 10^{-4} M solution of the laser dye rhodamine 101 in acidified ethanol experienced cooling when irradiated in the long wavelength tail of the absorption spectrum, contradictory to the problematic heating effects that are generated in other absorbing solutions. In view of the controversy surrounding this observation[11,12] it is important to discuss the difficult photophysics of the laser-cooled solution. In this paper a full description of the photophysical properties of this dye when pumped into the long wavelength wing of the absorption profile is presented. However, additional observations discussed in this work are the wider range of wavelengths over which the cooling effect has been shown to operate and the increased rate of cooling effected when the laser is tuned to 615 nm.

Background

The absorption of light by a molecule in solution creates an excited state that is deactivated by both radiative and nonradiative decay routes. The nonradiative route ultimately leads to an increase in thermal energy and in extreme cases a rapid rise in the sample temperature. However in molecules with a quantum efficiency of unity there is no nonradiative decay route and hence no mechanism for thermal input from this path. Generally, radiative decay from an excited state takes place from a vibrational level below the one that is excited directly, resulting in a large Stokes loss. The difference in energy is taken up by rapid vibrational relaxation in both the excited and ground states to produce a thermalized state after both excitation and emission. While this heating effect is smaller than that produced by nonradiative decay, the effect can still be substantial.

An alternative radiative decay route is implemented if a molecule is excited into the long wavelength tail of the absorption spectrum when the majority of the luminescence is anti-Stokes shifted from the excitation wavelength.[13,14] The source of this higher energy, anti-Stokes luminescence is attributed to the excitation of dye molecules populating high vibrational states, commonly termed "hot band" absorption. The dynamics of such S_1-S_0 relaxation have been successfully modeled by Blau.[15] Since energy must be conserved, a molecule that decays by a radiative path, to produce luminescence to higher energy than that of the absorbed light, must be at the expense of an alternative energy source in the system. The only other available energy source is thermal energy, and so an

S1089-5639(98)00589-1 CCC: $15.00
Published on Web 05/22/1998

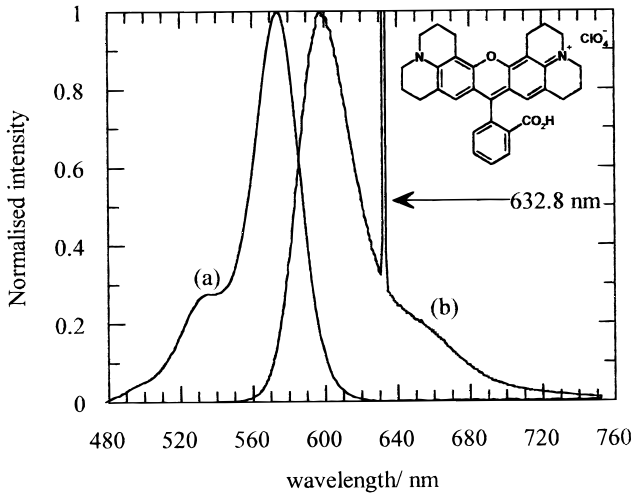

Figure 1. Normalized absorption spectrum (a) and corrected, dispersed emission spectrum (b) of a 2.5×10^{-7} M solution of rhodamine 101 in acidified ethanol. The inset shows the structure of the cationic form of rhodamine 101.

adiabatic system would be expected to show a concomitant decrease in temperature. Such is the case for a solution of rhodamine 101 in acidified ethanol when excited in the red, to lower energy than the 0−0 band origin. Such a solution has been shown to possess a unit luminescence quantum efficiency; indeed it is often used as a molecular quantum efficiency standard.[16] The implementation of a dye with a unit quantum efficiency has the beneficial effect of keeping the amount of triplet states to an absolute minimum and thus reduce the possibility of long-term photodegradation of the dye. Rhodamine 101 is also a well-known laser dye, indicating the absence of any transient absorptions in the spectral region of the emission spectrum. This is an important feature, as multiple-photon absorptions into higher excited states would decay nonradiatively to the first excited state and input thermal energy into the system.

Prior to any attempt to corroborate the existence of such a laser-cooling mechanism operating in an ethanolic rhodamine 101 solution, preliminary red edge excitation photophysical studies had to be performed. Firstly, knowledge of the positions of energy levels in the molecular system was required. More importantly, confirmation of the quantum efficiency of the solution being unity at higher concentrations than those quoted in the literature and the establishment that the frequency up-conversion mechanism operates via a one-photon path were also needed. From a measurement point of view, a further prerequisite is a nonintrusive temperature sensor. The experiments carried out to investigate these essential properties are described and the results presented in the following sections.

Absorption and Emission Spectra

In the laser-cooling experiment, the sample consisted of a 10^{-4} M solution of rhodamine 101 in acidified ethanol. The acidification of the dye was necessary since in polar solvents like ethanol the carboxyl group participates in a typical acid−base equilibrium between a cationic and zwitterionic form. In neutral solvents it is usual for both forms of the dye to be present. However, a uniform solution is obtained on addition of a small amount of acid or base, that of the cation on addition of acid and the zwitterion on the addition of base. The structure of the cationic form of R101 used in this work is shown in Figure 1. The principle absorption band of such a sample is intense ($\epsilon_{max} = 125\,700$ dm^3 mol^{-1} cm^{-1}) and narrow and corresponds to the $0 \leftarrow 0$ vibronic origin of the $S_0 \rightarrow S_1$ electronic transition ($\lambda_{max} = 575$ nm). The blue edge shoulder at $0 \leftarrow 0 + 1300$ cm^{-1} (532 nm) is associated with the $1 \leftarrow 0$ vibronic band in the totally symmetric breathing mode, and another weaker shoulder corresponds to the $2 \leftarrow 0$ vibronic band of the same $S_0 \rightarrow S_1$ electronic transition. The dependence on temperature of the absorption spectrum is shown in Figure 2. The spectra can be seen to narrow and increase in intensity for both the main band and the higher energy shoulder as the temperature is decreased. Isosbestic points at 589.2 ± 0.4, 565.0 ± 0.2, 544.5 ± 0.2, 520.0 ± 0.5, and 509.0 ± 0.5 nm are also observed.

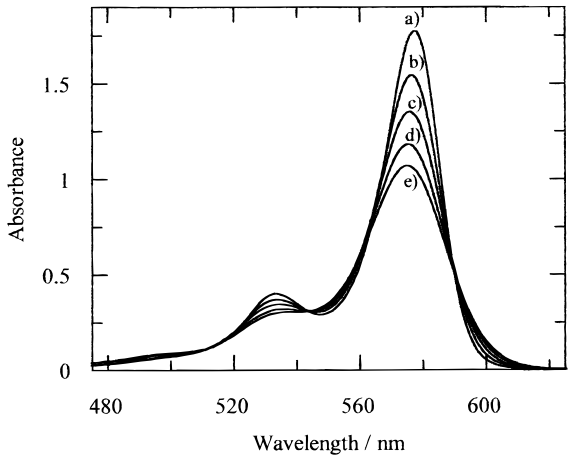

Figure 2. Temperature dependence of the absorption spectra of 10^{-4} M rhodamine 101 in acidified ethanol solution: (a) 140 K, (b) 180 K, (c) 220 K, (d) 260 K, and (e) 300 K.

The spectral narrowing and the intensity increase can be explained by the Boltzmann distribution function given in eq 1, where n_i is the population of the state with energy E_i, n_0 is the population of the lowest energy state, k_B is the Boltzmann constant, and T is the temperature of the system.

$$\frac{n_i}{n_0} = e^{-E_i/k_B T} \tag{1}$$

The Boltzmann distribution function predicts that most molecules will tend to lie in the lowest possible state at low temperatures, whereas at very high temperatures the distribution over energy states tends to be more uniform.

The emission spectrum of a 2.5×10^{-7} M solution of rhodamine 101 in acidified ethanol when excited at 632.8 nm is also shown in Figure 1. The spectral profile closely resembles the mirror image of the absorption spectrum, which is indicative of a close symmetry between the nuclear geometry of the ground- and excited-state species and lends credibility to the idea of high molecular rigidity. An estimate for the "true" isolated molecular $0 \leftarrow 0$ vibronic band origin is often taken as the energy of the overlap point of the normalized absorption and emission spectra. For rhodamine 101, this occurs at a wavelength of 586 nm.

The Origin of Anti-Stokes Luminescence

The generation of anti-Stokes luminescence from organic dyes itself is not a new discovery.[13,17,18] In the sample solution of rhodamine 101 in ethanol used in this study, this manifested itself as a yellow fluorescence when excited with red light from a helium−neon laser at 632.8 nm. Excitation at this wavelength occurs into the low-energy tail of the rhodamine 101 absorption spectrum and is 1262 cm^{-1} lower in energy than the 0−0 band origin at 586 nm and even 965 cm^{-1} lower in energy than the

emission maximum at 598 nm. This observed emission profile has the same shape and location as the conventional Stokes emission spectrum. The unusualness of these energy separations is shown in Figure 1, where the sharp peak at 632.8 nm is the scattered exciting light.

When R101 is excited in the red, long wavelength tail of the S_0-S_1 transition, beyond the emission peak, only a fraction of the molecules are interacting with the exciting laser light. This being the case, there are three possible models that could explain the origin of such "frequency-upconverted" luminescence.[13]

In the first model, absorption of a photon induces a transition from the lowest vibrational level of the ground singlet state S_0 to the lowest triplet state T_1. Since the triplet state is long-lived, the first excited state S_1 can be populated by thermal activation of the triplet state T_1, i.e., a similar mechanism to E-type delayed fluorescence. Temperature-dependent luminescence should be observed from the singlet and triplet levels. The lifetime of the luminescence should be equal to the lifetime of the triplet state, and the absorption coefficient should be largely independent of temperature.[13]

In the second model, absorption of a photon induces a transition from one of the many vibrational levels of the ground singlet state S_0 to the lowest vibrational level of the first excited state, S_1. Since the energy of the absorbed quanta is less than the energy difference of the 0−0 transition, the levels of S_0 involved are some 1000 cm^{-1} above the lowest vibrational level of S_0. The absorption coefficients should be strongly temperature dependent because the populations of these levels of S_0 are determined by the Boltzmann distribution. Strong temperature dependent luminescence should be observed only from $S_1 \rightarrow S_0$ transitions.

In the final model, the first excited singlet state is populated by a two-photon absorption process inducing transitions from S_0 to S_1 and S_2. The S_1 can then fluoresce back down to the ground state.[19] The absorption and fluorescence would both be predominantly independent of temperature, and the fluorescence intensity related to the square of the excitation intensity.

To determine which mechanism is responsible for the anti-Stokes fluorescence production, experiments were carried out to distinguish between the models.

From a simple rate equation model[20,21] it can be deduced that the frequency-upconverted luminescence intensity I_u will be proportional to the power n of the excitation intensity I_e; thus, $I_u \propto I_e^n$. It should be noted, however, that the model takes no account of depletion of the ground-state populations, so that in general a nonintegral value of n can be expected and the effect may even saturate. The dependence of the yellow luminescence intensity at 620 nm on the excitation intensity at 634 nm is shown in Figure 3a and the logarithm of these data shown in Figure 3b. From the second plot the value of n is determined as 0.98, which is very close to 1 and so only one photon is involved in the upconversion process. Two-photon absorption is quadratic in the intensity of the exciting light ($n = 2$), suggesting that the two-photon absorption model is not a viable explanation for the mechanism of the yellow luminescence production.

Figure 4 shows the temperature dependence of the anti-Stokes fluorescence spectrum exciting with 632.8 nm light from a He−Ne laser. The emission is observed to decrease as the temperature of the solution decreases. Similar dependencies were found for all such long wavelength excitations in the 610−660 nm region. The lack of temperature dependence of the emission spectra, required by model 3, acts as a corollary to

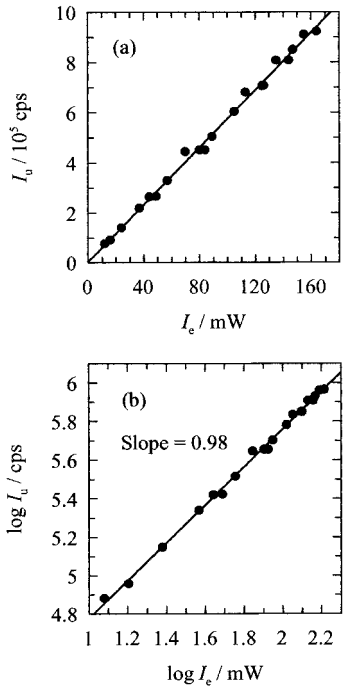

Figure 3. Experimental measurements of (a) the linear dependence of the fluorescence signal at 620 nm, with input power, and (b) the logarithmic plot of the same data showing a linear dependence of slope 0.98 (cps = counts per second).

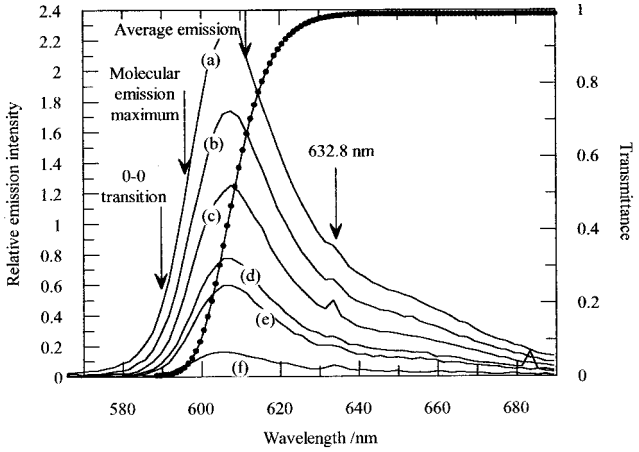

Figure 4. Dispersed emission spectra of a 10^{-4} M solution of rhodamine 101 in acidified ethanol in a cylindrical cell at (a) 310 K, (b) 290 K, (c) 270 K, (d) 250 K, (e) 220 K, and (f) 200 K. Also shown is the transmission of the low-energy absorption tail of this sample, the 1 mW He−Ne excitation wavelength, the position of the average wavelength of the measured emission spectrum (610 nm), the position of the average energy of the molecular emission spectrum (595 nm), and the position of the 0−0 band origin (590 nm).

the linear relationship between emission and excitation intensity in eliminating the two-photon absorption process as being a source of the upconverted luminescence.

The dependence on temperature of the emission data does not distinguish between models 1 and 2. This was achieved by a study of the lifetime of the yellow luminescence using a time-correlated single-photon counting apparatus using pulsed dye laser excitation at 630 nm. The decay time of a rhodamine 101 in acidified ethanol solution was found to be 4.1 ± 0.1 ns. Measurements of the triplet lifetime of similar dyes[22] in oxygen-saturated solutions yield triplet-state lifetimes of $\tau_T \approx 10^{-7}$ s. The lifetime of the luminescence must be equal to the triplet lifetime if model 1 is applicable.

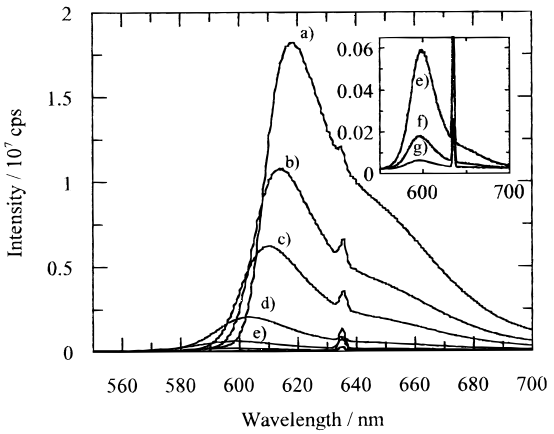

Figure 5. Concentration dependence of the fluorescence emission spectra on R101 in acidic ethanol: (a) 2.45×10^{-4} M, (b) 1.22×10^{-4} M, (c) 6.16×10^{-5} M, (d) 1.55×10^{-5} M, (e) 4.00×10^{-6} M, (f) 1.04×10^{-6} M, and (g) 2.28×10^{-7} M.

The frequency upconversion mechanism responsible for the production of the anti-Stokes fluorescence is therefore attributed to the excitation of dye molecules, populating high vibrational states in S_0, into the first singlet excited state S_1, a process known as "hot band absorption". While the absorbance at 632.8 nm cannot be readily measured, the sensitivity of fluorescence spectroscopy demonstrates that it is finite. The origin of the weak absorption is due to the small but finite population of energy states 1262 cm^{-1} above the lowest vibrational level of the electronic ground state, S_0. The Boltzmann distribution in eq 1 predicts the relative population of the energy states 1262 cm^{-1} above the 0−0 level to be 2.11×10^{-3}. Even though the effective concentration of available rhodamine molecules at 632.8 nm is low, the unit quantum efficiency of rhodamine and high molar absorption coefficient make a sufficiently high detection efficiency of fluorescence to enable the existence of the weak absorption to be detected.

Determination of Quantum Efficiency at High Concentration

Published data on the absorption behavior of alcoholic rhodamine solutions at high concentration are in general agreement that shifts in the absorption spectra caused by dye aggregation[23−25] do not occur until the solution concentration exceeds 5×10^{-3} M. Absorption studies on solutions of rhodamine in acidic ethanol up to this limiting concentration did not show any deviation from the Beer−Lambert law, similar to other rhodamine dyes. It was therefore concluded that at concentrations below 5×10^{-3} M, molecules of rhodamine were solvated as monomers in acidic ethanol. However, confirmation of the absence of aggregation at the laser-cooling concentration of 10^{-4} M was insufficient to clarify that the molecular fluorescence quantum efficiency, ϕ_f, of such a concentrated solution was unity, as has been shown to be the case in less concentrated solutions[16] (below 10^{-5} M).

Figure 5 displays the fluorescence spectra of rhodamine 101 in acidic ethanol when excited at 635 nm. As the concentration of dye increases, the emission spectrum increases in intensity with a shift in the emission maximum to longer wavelengths and an overall change in spectral shape. The Stokes shift for an acidic ethanolic rhodamine 101 solution is small (669 cm^{-1}), and thus the overlap of the absorption and emission spectra is large. It is this overlap that indirectly facilitates the red shift in the emission spectra observed at higher concentrations by means of reabsorption or the so-called "inner filter effect". This effect is due to the absorption of some of the incident light before it reaches the point in the sample from which luminescence is observed ("primary" inner filter effect) and reabsorption of some of the emitted light before it leaves the cell and reaches the detector ("secondary" inner filter effect).

An experimental approach that allows simultaneous correction for both the primary and secondary inner filter effects is the "diagonal cell shift" method where fluorescence intensities are measured at two points along the cell diagonal.[26] The intensities of the emitted radiation, at any particular wavelength, I_1 and I_2, from these two points can be expressed according to eqs 2 and 3, where I_0 is the undistorted spectral intensity, D_x and D_m are the optical densities at the excitation and emission wavelengths, respectively, and l_1 and l_2 are the depths into the solution from which the two emission spectra originate.

$$I_1 = I_0 \times 10^{-D_x l_1} \times 10^{-D_m l_1} = I_0 \times 10^{-(D_x + D_m) l_1} \quad (2)$$

$$I_2 = I_0 \times 10^{-(D_x + D_m) l_2} \quad (3)$$

From these equations it can be deduced that

$$D_x + D_m = \log(I_1/I_2)/(l_2 - l_1) \quad (4)$$

which leads to

$$I_0 = I_1 (I_1/I_2)^{l_1/(l_2 - l_1)} \quad (5)$$

where l_1 and l_2 are geometry-dependent constants, so that the expression $l_1/(l_2 - l_1)$ can be replaced by a single geometry dependent parameter a. Equation 5 then becomes simply

$$I_0 = I_1 (I_1/I_2)^a \quad (6)$$

An experiment implementing this theory was carried out by irradiating the sample held in a 1 cm cuvette mounted on a precision x,y translation stage. The irradiating beam was set up in a stable configuration to excite the sample fluorescence at a specific depth l_1 or l_2 in the sample by focusing with a 5 cm focal length lens. l_1 and l_2 were selected by translating the cell along its diagonal with respect to the exciting beam. The fluorescence was detected perpendicular to the exciting light and focused onto the slits of a 1 m monochromator. This light was subsequently detected by a photomultiplier tube connected to a gated photon counter interfaced to a computer for data analysis. At each change in cell position, the focusing of the fluorescence on the slits of the monochromator was optimized.

The diagonal cell shift method was applied to solutions of rhodamine 101 in acidified ethanol over the concentration range 10^{-7}−10^{-3} M when excited at 622, 635, and 650 nm. For each concentration and excitation wavelength the profile of the real emission intensity at each wavelength, I_0, was calculated using eq 6. It was reasonable to assume that the quantum efficiency of the 10^{-7} M solution was unity.[16] The relative fluorescence quantum efficiencies of the more concentrated solutions were then calculated by ratioing the real fluorescence areas normalized to the concentration with that of the 10^{-7} M solution. A graphical summary of these data is shown in Figure 6. It can therefore be deduced that when excited in the red, the quantum efficiency of a solution of rhodamine 101 in acidified ethanol is independent of the excitation wavelength, but more importantly, the concentration at which the quantum efficiency "appears" to become less than unity is identical for all

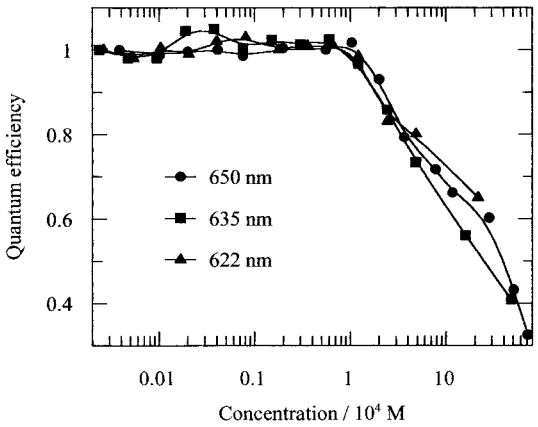

Figure 6. Dependence of the fluorescence quantum efficiency of rhodamine 101 in acidified ethanol on concentration, calculated using the diagonal cell shift correction method, when excited at 650 nm, 635 nm, and 622 nm.

wavelengths: a concentration greater than that used in the laser cooling experiment. At concentrations greater than this turning point, either the quantum efficiency of the solution has really decreased from unity, or the extent of the inner filter effect has become so large that the diagonal cell shift method can no longer correct for the severe spectral distortions.

Feasibility Study

Prior to conducting any investigative laser-cooling experiment a thermodynamic model of the system was made to estimate the magnitude of the temperature change expected and the time taken to effect such a change. Variable parameters introduced into the equation are container mass, sample volume, concentration, heat capacity, the irradiating power and wavelength, and the radiative heat load from the sample surroundings.

The fluorescence upconversion data shown in Figure 4 were obtained using the 632.8 nm excitation from a 1 mW He−Ne. The sample was 0.3 mL of a 10^{-4} M solution of rhodamine 101 in degassed acidified ethanol (10^{-2} M HCl) contained in a 3.1 g, sealed cylindrical quartz container.

In the case of rhodamine 101, where there are no nonradiative relaxations from the excited state to ground state, the applied power, P_{applied}, is proportional to both the absorbed pump power and the average difference in the photon energies of the pump and emitted radiation. In terms of the wavelength of the pump radiation, λ_{pump}, the applied power is

$$P_{\text{applied}} = P_{\text{pump}} \frac{\lambda_{\text{pump}}}{hc}[1 - 10^{-\text{ABS}}]hc\left[\frac{1}{\lambda_{\text{pump}}} - \frac{1}{\lambda_{\text{ave}}}\right] \text{J s}^{-1} \quad (7)$$

The first term, $P_{\text{pump}}(\lambda_{\text{pump}}/hc)$, in eq 7 represents the number of photons reaching the sample per second. P_{pump} is the power of the exciting light expressed in J s^{-1}, λ_{pump} is the wavelength of the exciting light expressed in meters, h is Planck's constant, and c is the speed of light. The fraction of the photons reaching the sample that are actually absorbed to excite the fluorescence is expressed by the second term, $1 - 10^{-\text{ABS}}$, where ABS is the optical density and $10^{-\text{ABS}}$ the transmittance of the sample at the excitation wavelength, λ_{pump}. In the final term, $hc[1/\lambda_{\text{pump}} - 1/\lambda_{\text{ave}}]$, the amount of thermal energy, expressed in joules, removed per absorbed photon is calculated. λ_{ave} is the wavelength, in meters, of the average energy of the light emitted from the sample. If $\lambda_{\text{pump}} < \lambda_{\text{ave}}$, the sample is heated and P_{applied} is a positive quantity; that is, heat flows into the sample. Conversely, if $\lambda_{\text{pump}} > \lambda_{\text{ave}}$, then the sample is cooled, with heat flow from the sample, and P_{applied} is a negative quantity.

Counteracting the applied power is the heat load from the sample surroundings, P_{load}, which in this experiment is from the radiative coupling between the walls of the cryostat (Oxford Instruments DN 1704) that are at ambient temperature T_C. With the sample at temperature T_S, the radiative coupling is given by[27]

$$P_{\text{load}} = \sigma \frac{A_S}{\frac{1}{\epsilon_S} + \frac{A_S}{A_C}\left(\frac{1}{\epsilon_C} - 1\right)}(T_C^4 - T_S^4) \quad (8)$$

where ϵ_S and ϵ_C are the sample emissivities over the wavelength range, relevant to a room-temperature body, for the sample and chamber respectively. σ is the Stefan−Boltzmann constant; A_S and A_C are the sample and chamber surface areas, respectively. The expressions for P_{applied} and P_{load} can be simplified (see Appendix A) and summed to give the total power, P_{total}, given by eq 9.

$$P_{\text{total}} = P_{\text{pump}}[1 - 10^{-\text{ABS}}]\left[\frac{\lambda_{\text{ave}} - \lambda_{\text{pump}}}{\lambda_{\text{ave}}}\right] + 4\sigma \frac{A_S}{\frac{1}{\epsilon_S} + \frac{A_S}{A_C}\left(\frac{1}{\epsilon_C} - 1\right)} T_C^3 (T_C - T_S) \quad (9)$$

The change in temperature of the sample can be shown (see Appendix A) to be related to the applied power, P_{applied}, and the sample heat capacity, C_V, by

$$T_C - T_S = (T_C - T_{S,t=0}) \exp^{-kt} + \frac{P_{\text{applied}}}{kC_V}(\exp^{-kt} - 1) \quad (10)$$

where $T_{S,t=0}$ is the sample temperature at time $t = 0$, C_V is the sample heat capacity at constant volume and k is defined as

$$k = 4\sigma \frac{A_S}{\frac{1}{\epsilon_S} + \frac{A_S}{A_C}\left(\frac{1}{\epsilon_C} - 1\right)} \frac{T_C^3}{C_V} \quad (11)$$

The sample consisted of 0.3 ml of a solution of 10^{-4} M rhodamine 101 in acidified ethanol (10^{-2} M HCl) in a fused silica, cylindrical tube (length 2 cm, diameter 0.6 cm). The solution was degassed by freeze−pump−thawing the sample at low pressure, sealed off, and then placed in the cryostat. By referring to Figure 4, the absorption of the example solution at, for example, 632.8 nm was 0.02 and the measured average wavelength of the emission, λ_{ave}, determined to be 610 nm. With ABS = 0.02, λ_{pump} = 632.8 nm and λ_{ave} = 610 nm, and substituting these values into the first term in eq 9 returns a value for P_{applied} of -0.17×10^{-3} J s^{-1} per 100 mW of pump power, P_{pump}. The negative sign indicates that the sample temperature will be lowered upon irradiation at this wavelength.

The heat capacity of the sample is the sum of that of the solvent and the container assuming that the contribution made by the rhodamine 101 molecules is negligible. Ethanol has a molar heat capacity of 111 J K^{-1} mol^{-1} and a density of 0.789 g ml^{-1}; thus, a 0.3 mL sample of rhodamine 101 in acidified ethanol has a heat capacity of 0.573 J K^{-1}. The heat capacity of quartz is 0.78 J K^{-1} g^{-1}; thus, the combined heat capacity of the sample and container is ca. 3 J K^{-1}. The sample has an approximate area, A_S, of 4 cm^2 and an emissivity, ϵ_S, of ca.

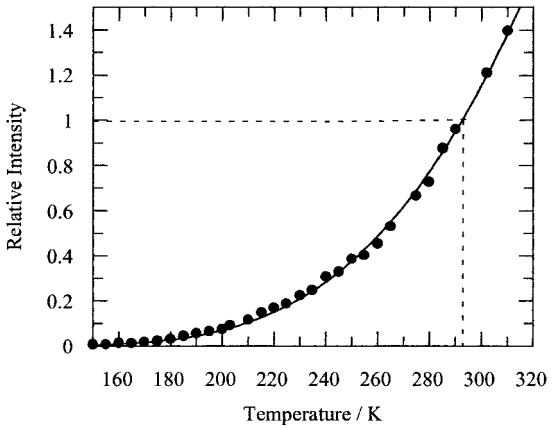

Figure 7. Dependence of the fluorescence intensity at 620 nm on temperature, for a 10^{-4} M rhodamine 101 in acidified ethanol solution. The fluorescence intensity is normalized to that at room temperature (292.4 K). The solid line represents an experimental fit to the function: Relative intensity, $I = 310 \exp(-2.31 \times 10^{-20}/k_B T)$.

0.7. The inside of the cryostat is of highly polished stainless steel ($\epsilon_S \approx 0.02$) with four fused silica optical windows. Estimating the emissivity of the chamber to be ca. 0.05 with an area of ca. 15 cm^2 gives a value for the constant k of 1.15×10^{-4} s^{-1}. Substituting this value into eq 10 along with a value for $P_{applied}$ of -0.34×10^{-3} (200 mW at 632.8 nm) and an initial sample temperature equal to the surrounding, $T_{S,t=0} = T_C = 292.4$ K, predicts that the sample temperature will drop, reaching an equilibrium value of 291.9 K after ~700 min. For the first 50 min the temperature will drop linearly at a rate of approximately 3×10^{-3} K min^{-1}. Using the sensitive, anti-Stokes fluorescence as a method of determining the sample temperature, discussed below, this change is easily measurable.

Temperature Calibration

The data plotted in Figure 5 show the temperature dependence of the emission spectra from the sample. In addition to confirming the origin of the anti-Stokes luminescence, these data also provide an ideal method for monitoring the temperature of the sample since any change in temperature will induce an increase or decrease in the luminescence intensity depending on whether the sample is heated or cooled. This is very convenient, as other temperature measuring devices like thermocouples and thermistors have to be introduced into the sample as a foreign body that will act as a heat sink and raise the heat capacity of the system. A similar approach has also been adopted by Mungan et al.[8]

The temperature dependence of the emission of this sample was measured by supporting it in a cryostat and allowing it to equilibrate to a specified temperature. Light from a stable, 1 mW He−Ne laser was used to excite the sample at 632.8 nm and the luminescence collected perpendicular to the excitation with a 5 cm focal length lens that focused the light into the slits of a 1 m monochromator. This light was subsequently detected by a photomultiplier tube connected to a gated photon counter interfaced to a computer for data analysis. The dependence of the emission spectrum was calibrated over the temperature range 300−150 K.

The data plotted in Figure 7 show the temperature dependence of the luminescence intensity at 620 nm, taken from the data series shown in Figure 4 and can be modeled with a function of the form:

$$\text{relative intensity, } I = A \exp(-\Delta E/k_B T) \qquad (12)$$

where k_B is the Boltzmann constant and T is the temperature. ΔE was determined to have a value of 1166 ± 50 cm^{-1}, in good agreement, to a first approximation, with the difference between the excitation energy (15 803 cm^{-1}) and the band origin energy (16 978 cm^{-1}) as predicted by the Boltzmann distribution.

The inherent temperature sensitivity of the emission from a solution of R101 in ethanol provides an ideal method for monitoring the temperature of the sample. The temperature can be calibrated to an accuracy of better than 0.2 K. This feature proved to be extremely effective in monitoring the temperature of the sample during fluorescence "cooling" and "heating" experiments when the fluorescence signals at an emission wavelength of 620 nm were recorded. Conversion of these signals using the results of the fit to the data, presented in Figure 7, yields the temperature of the sample, although over the small temperature region studied in the laser cooling experiments, the dependence can be considered to be approximately linear. The predicted drop in intensity of 0.5 K, estimated in the feasibility study, corresponds to a drop in relative intensity of 1%, which represents a change that is easily detectable.

Laser Cooling

The sample (0.3 mL of degassed 10^{-4} M rhodamine 101 in acidified ethanol) was first attached to a Teflon holder, to eliminate conduction, and then suspended in the cryostat (Oxford Instruments DN1704), which was subsequently evacuated to a pressure of $<10^{-4}$ mbar, to eliminate convection, and the temperature controller disabled. The cryostat was then returned to the luminescence spectrometer described previously with the He−Ne laser set up in a stable configuration to excite luminescence and monitor any changes in temperature by the changes in intensity. The output from a continuous wave dye laser provided the pump beam which was focused into the sample using a 5 cm focal length cylindrical lens, coaligned with the monitoring He−Ne beam, but passing through the sample in the opposite direction. Up to 350 mW of pump light in the wavelength range 580−680 nm was available using either rhodamine 6G or Kiton Red as the laser gain dyes, pumped with the 3 W all-line output from an argon ion laser. Temperature measurements were made at 15 min intervals by momentarily blocking the pump laser, to extinguish the intense luminescence generated, and measuring the luminescence intensity at 620 nm when excited by the stabilized He−Ne laser. Pump beam irradiation was continued for periods up to 4 h. After this time, the luminescence signal was continued to be monitored, until the signal returned to its initial value at time zero. In addition, luminescence from the sample was also monitored without any irradiating light from the dye laser, in order to provide a reference signal and judge long-term stability of the sample temperature.

Two examples of raw data are plotted in Figure 8 with the data normalized to the luminescence intensity at time zero. These represent the data recorded over a 4 h period at pump wavelengths of 583 and 634 nm, 27 nm below and 24 nm above λ_{ave}, respectively, as well as the reequilibration of these signals to the time zero value. When irradiating at 583 nm the luminescence intensity clearly increases, while irradiating at 634 nm the signal decreases. In both cases the signal eventually returns to the time zero value after ceasing dye laser excitation, indicating no long-term degradation of the dye. Absorption spectra recorded prior to and following the 4 h intense pumping were also measured and found to be identical, again eliminating the possibility of degradation. It is therefore concluded that

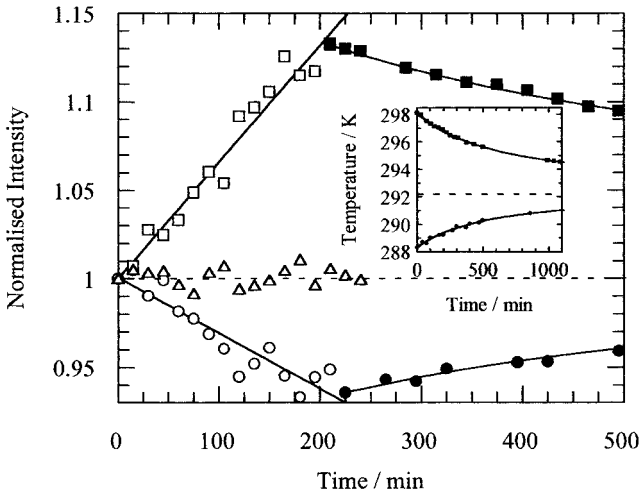

Figure 8. Dependence of the emission intensity at 620 nm, monitored with time, when excited at (□) 583 nm (170 mW) and (○) 634 nm (380 mW), for ≈220 min. The data ■ and ● represent the radiative coupling of the sample with the surroundings. The data △ are a reference. The inset shows the radiative coupling data over a longer time period, converted to the temperature scale, modeled with eq 13.

the change in luminescence intensity is a result of a change in temperature of the sample caused by laser irradiation. At 583 nm the sample is heating up, while at the longer wavelength, 634 nm, the sample is cooling down. This constituted the first direct observation of the cooling of a liquid-phase sample with the use of laser light and proved the postulate to be true.[10,12]

In Figure 8, in addition to the 583 and 634 nm excitation luminescence data, a reference set of data is also plotted where the He−Ne stimulated luminescence from the sample was monitored without any intermediate irradiating light from the dye laser. This reference signal remains unaffected over a 4 h period, eliminating the possibility of thermal drifts in the cryostat as instigating the observed temperature change in the sample.

Comparison of the change in luminescence intensity with the calibration data shown in Figure 7 suggests that the 5% reduction in intensity in 220 min results from of a drop in temperature of 3.0 ± 0.5 K. The predicted applied power, $P_{applied}$, when exciting with 380 mW at 634 nm is -6.73×10^{-4} J s^{-1}. Substituting this power into eq 10, with the estimated value for the characteristic rate constant for radiative coupling, k, of 1.15×10^{-4} s^{-1} and the initial conditions, $T_{S,t=0} = T_C = 292.4$ K predicts that the sample will reach an equilibrium temperature of 290.5 K, a drop of only 1.9 K. After 220 min, it also predicts that the temperature will have dropped by only 1.5 K to 290.9 K. Conversely a 13% increase in intensity corresponds to a 7 K rise in temperature, that observed when the sample is irradiated with 170 mW of laser light tuned to 583 nm. This value is less than that predicted by eq 10, which suggests (again using $k = 1.15 \times 10^{-4}$ s^{-1} and $T_{S,t=0} = T_C = 292.4$ K) that in a 220 min period the temperature will rise exponentially by 17 K. Apart from the predicted change in temperature, the most noticeable difference between the prediction of the feasibility study and experiment is the functional form of the temperature change. The experimental data show only a linear trend, while the prediction is an exponential one, a discrepancy that can be rationalized in terms of a smaller characteristic rate constant, k. Equation 11 defines this constant in terms of the emissivities and surface areas of the sample and surroundings. By removing the applied power and allowing the sample to thermally

TABLE 1: Calculation of the Observed $P_{applied}$ at All Experimental Excitation Wavelengths. The Fraction $P_{applied}/P_{pump}$ Is the Normalization of $P_{applied}$ to That Observable from a 1 mW Laser of the Same Pump Wavelength

λ_{pump} (nm)	P_{pump} (mW)	10^{-ABS}	dT/d(time) (K min^{-1})	$P_{applied}$ (mW)	$100(P_{applied}/P_{pump})$ (mW)
583	170	2×10^{-13}	0.0428	2.14	1.26
595	130	5×10^{-5}	0.0360	1.80	1.38
605	310	0.081	0.0631	3.16	1.10
610	280	0.314	0.0039	0.20	0.07
615	200	0.589	−0.0148	−0.74	−0.37
620	250	0.785	−0.0103	−0.51.	−0.21
634	380	0.961	−0.0133	−0.66	−0.19
652	200	0.995	0.0030	0.15	0.05

reequilibrate with the surroundings, it is possible to determine this constant experimentally. Figure 8 shows that for the first 300 min the recovery is linear, although when extended to 1000 min (see inset to Figure 8), the nonlinearity becomes apparent. The solid lines in the inset of Figure 8 are found by modeling these data with the function (Appendix A, eq A9), and return a

$$T_C - T_S = (T_C - T_{S,t=0}) \exp^{-kt} \tag{13}$$

common value for the characteristic rate constant k of $(3.3 \pm 0.7) \times 10^{-5}$ s^{-1} for both the heating and cooling data. This is only a factor of 3.5 times smaller than predicted in the feasibility study, suggesting that the emissivities and surface areas chosen were slightly incorrect. The discrepancy is almost certainly due to the properties of the interior of the cryostat. Reducing the emissivity of the inner surface to 0.025 and the surface area to 10 cm^2 returns a value of k of 3.5×10^{-5} s^{-1}, a value that is more consistent with the value derived experimentally. A reduced value of k also explains why the temperature changes linearly for both the heating and cooling experiments. For small values of kt, the temperature change can be approximated (Appendix eq A10) by

$$T_C - T_S \cong \frac{-P_{applied}}{C_V} t \tag{14}$$

Using this relationship, the gradients of the heating and cooling data in Figure 8 give the experimental values of $P_{applied}$ from the gradients. These data are presented in Table 1.

The results of a more systematic investigation of the temperature change induced by pumping at different wavelengths in the 580−660 nm region are shown in Figure 9. The results complement the previously published data[10] when exciting at 583, 605, 620, and 634 nm; when exciting to higher energies than λ_{ave}, at 610 nm, the sample endures a heating, and when pumping to lower energies than λ_{ave}, the sample experiences cooling. When the dye laser is tuned to λ_{ave}, the mean photon energy, no appreciable change in the temperature occurs. At this unique pump wavelength the absorbed and emitted powers exactly balance so that eq 7 returns a value of zero for $P_{applied}$ ($\lambda_{pump} = \lambda_{ave}$). The implication of this negating of heat flow into or out of the sample is that the sample will remain at the surrounding temperature, T_C, throughout the laser irradiation, a postulate that is observed to be validated in the experiment. This finding is perhaps a more meaningful reference than that when the pump laser is shut off and the luminescence intensity monitored solely by the He−Ne. It eliminates potential flaws in the laser-cooling experiment and substantiates previous evidence[12] to reject photodegradation[11] as being the origin of the decrease in luminescence intensity.

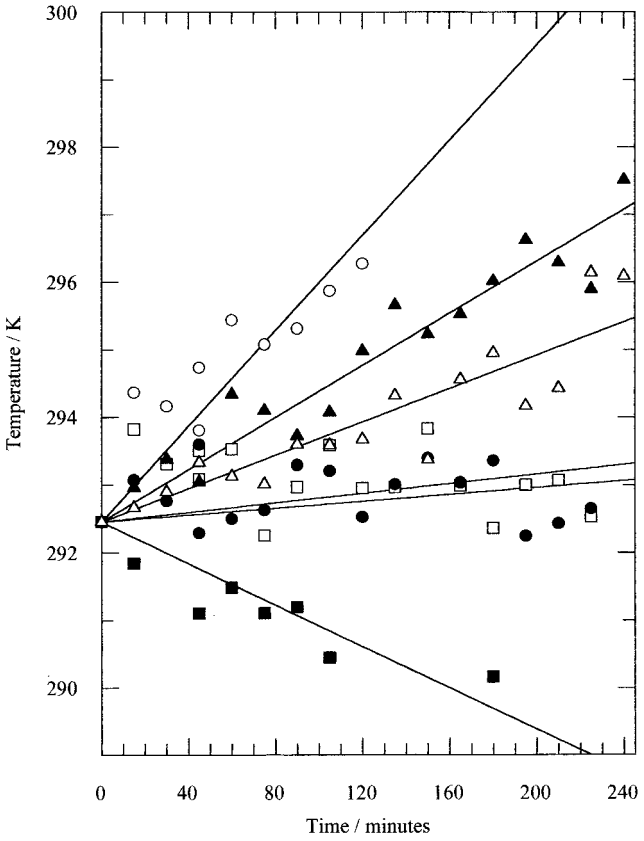

Figure 9. Dependence of the sample temperature with time when (a) a 10^{-4} M rhodamine 101 in acidified ethanol solution is excited at (○) 595 nm (130 mW), (□) 610 nm (280 mW), (■) 615 nm (200 mW), and (●) 652 nm (320 mW) and (b) when a 10^{-3} M solution of rhodamine 101 in acidified ethanol is excited at (▲) 610 nm (250 mW) and (△) 656 nm (260 mW). Solid lines are a linear fit to the data from which $P_{applied}$ is calculated.

For each set of data presented in Figure 9, the gradients of the linear fits signify the rate of temperature change per min encountered by the sample under sustained irradiation at the specified laser power. From these gradients, a conversion to K min^{-1} allows the observed applied power, $P_{applied}$, to be calculated by multiplying with the 3 J K^{-1} heat capacity of the sample. These values are shown in Table 1. The ratio ($P_{applied}/P_{pump}$) normalizes the variation in the pump powers, so that 100-($P_{applied}/P_{pump}$) represents the applied power (in mW) in an equivalent experiment that pumping with $P_{pump} = 100$ mW would give.

From the cooling powers, corrected for pump power, it can be seen that there is a clear trade-off between lowering the energy of the incident light to extract more energy per absorbed photon and the number of absorbed photons. The most efficient cooling of the sample is induced when the pump laser is tuned to 615 nm. This observation is better represented in Figure 10, where the applied power induced by a 100 mW pump laser is plotted for the experimental excitation wavelengths. The values between 614 and 635 nm are less than zero, corresponding to cooling. The solid plot is that of the predicted applied power for this 100 mW laser power calculated from eq 7. Comparison of the theoretical $P_{applied}$ with the experimental values reveals that at λ_{ave} and in the long wavelength cooling regime the observed results do not, within experimental error, differ by more than 0.1 mW from that predicted. The large discrepancy between prediction and observation in the heating

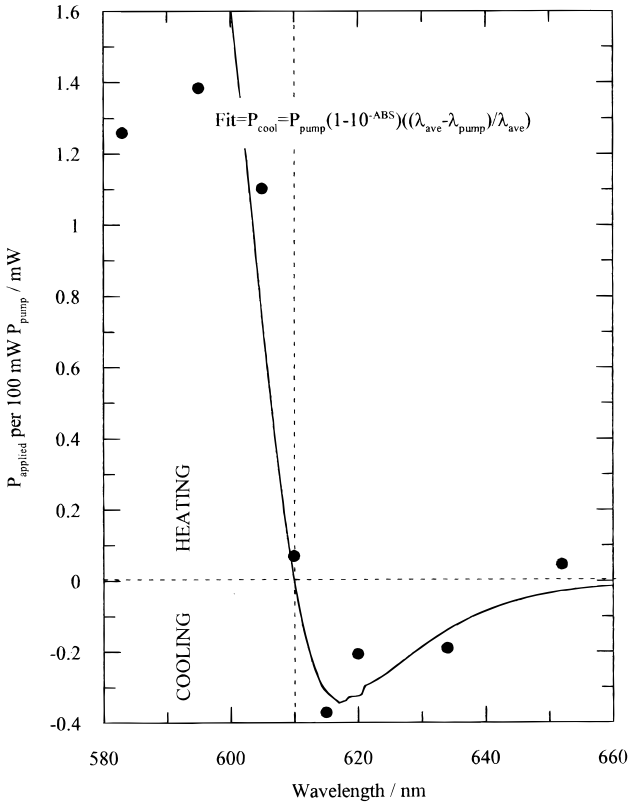

Figure 10. Amplitudes (●) of the applied power, $P_{applied}$, per 100 mW of pump laser power as a function of irradiating wavelength for a 10^{-4} M solution of rhodamine 101 in acidified ethanol. The solid curve (—) is a plot of the predicted $P_{applied}$ for 100 mW of exciting light assuming $\phi = 1$ calculated using eq 9.

domain requires more justification. At the two wavelengths, 583 and 595 nm, the sample absorbance is high, and thus eq 9 reduces to

$$P_{total} \approx P_{pump}\left[\frac{\lambda_{ave} - \lambda_{pump}}{\lambda_{ave}}\right] + kC_V(T_C - T_S) \qquad (15)$$

The experimental data in Figure 9 exhibit a linear dependence with time, and it again must therefore be concluded that the radiative coupling is small with respect to the applied power (i.e., the second term in eq 15 can be ignored). This is consistent with the small characteristic coupling constant, *k*, determined earlier. Thus in order to rationalize the discrepancy between the predicted and experimentally observed powers, the average emission wavelength must be less than for the cooling experiment. At these two excitation wavelengths the penetration depth of the excitation light into the sample is small, and thus the emission emanates predominantly from close to the entry point. The effects of reabsorption[15,29,30] are much reduced, and therefore the average wavelength of emission is closer to that of the molecular emission (shown in Figure 5f). Although the absorbance of the sample in the cooling experiment is low, leading to the majority of the light traveling straight through the sample, the cooling effect close to the entry and exit points is also larger due to the reduced average wavelength of emission. By changing the average energy of emission to 587 and 600 nm, the predicted ratio, 100($P_{applied}/P_{pump}$), predicts the experimentally observed values of 1.26 and 1.38 for the pumping wavelengths of 583 and 595 nm, respectively. It is therefore not unreasonable to assume that the discrepancy between the experiment and theory for these two pumping wavelengths can

be readily explained in terms of a reabsorption effect. It is also recognized that at these two pumping wavelengths the heating effect should be considerable and lead to large increases in sample temperature, at which point the radiative coupling with the surroundings will become significant. However, the experimental data in Figure 9 are linear, and therefore this explanation cannot be justified.

The evidence presented so far clearly demonstrates that irradiation of a 10^{-4} M solution of rhodamine 101 in acidified ethanol at energies lower than the average emission energy leads to a cooling of the sample. A cooling rate of 3 K h^{-1} has been observed when pumping at 634 nm with 380 mW of CW laser light. Methods of enhancing this effect have been considered; perhaps the most obvious method would be to increase the concentration of rhodamine 101 in the solution: By implementing identical pumping and temperature monitoring techniques as used in the 10^{-4} M rhodamine 101 in acidified ethanol experiment, a 10^{-3} M solution of rhodamine 101 in acidified ethanol was excited in the 595−665 nm range. The average wavelength of emission of this solution was found to be 637 nm, red shifted when compared to the less concentrated solution due to the more prevalent reabsorption effect. If this solution were to display similar optical refrigeration effects, then these would be expected to occur when exciting at wavelengths longer than 637 nm. Figure 9 displays the measured temperature changes experienced by this 10^{-3} M solution when excited at 610 and 656 nm. The 610 nm data are seen to induce a rise in the sample temperature as expected; however, the 656 nm excitation data are also seen to induce a rise in the sample temperature. Such a result suggests that the fluorescence quantum efficiency of this solution is no longer unity, lending credibility to the results displayed in Figure 6, where a 10^{-3} M solution of acidic rhodamine 101 in ethanol was found have $\phi_f = 0.6$. Large molecules are well-known to form dimers and higher order aggregates at higher concentrations that do not luminesce.[15,28] The rapid nonradiative internal conversion processes in these species would therefore lead to sample heating and defeat the object of increasing the cooling effect.

Another method of enhancing this cooling effect would be to reduce the solution volume and the size of the container. However, a study of how the container size to volume ratio effects the cooling rate would have to be investigated since silica surfaces have been shown to enhance nonradiative decay for dye molecules in contact with or near the surface.[31] All these factors introduce a delicate balance between sample concentration, quantum efficiency, pump wavelength and power, and the ability to effect an observable cooling effect in the sample.

Conclusion

In conclusion, it has been shown that irradiation of a 10^{-4} M solution of rhodamine 101 in acidified ethanol at energies lower than the 0−0 band origin leads to a single-photon frequency up-conversion process. Cooling of the sample occurs when the irradiating frequency is tuned to lower energies than the average energy of the emitted light. This is in contrast to everyday experiences that tell us that when an absorbing body is irradiated with light, its temperature will rise. The effect of radiative coupling between the sample and surroundings has been found to be much less than that predicted by two black body radiators. This is due to the low emissivity of the mirrorlike interior of the optical cryostat used as our sample chamber, which justifies, in part, our original assumption of ignoring radiative coupling.[8,10,12]

To observe anti-Stokes luminescence cooling, a dye solution with a molecular fluorescence quantum efficiency very close to unity is required. Indeed, the cooling effect confirms the unit quantum efficiency of fluorescence. Furthermore the dye has to be extremely pure, and the intrinsic solvent absorption needs to be very small. The rate of the induced cooling effect also depends on the number of absorbing molecules at the pump wavelength, the energy separation of the pumping frequency from that of the average frequency of the fluorescence, and the number of photons exciting the sample per second. The magnitude of an observed temperature decrease is also dependent on the heat capacity of the solution and its container, which in turn is related to the volume of the sample.

In this work only solutions of rhodamine 101 in acidified ethanol were studied. However, other solutions that may be expected to show similar effects are 9,10-diphenylanthracene in cyclohexane[30] and other dyes of the xanthene family when solvated in glycerol.[28] These all have molecular quantum efficiencies of unity. In glycerol the viscosity is sufficiently high to prevent the planarity of the ground-state xanthene dye being lost before light emission takes place, so that structural mobility is eliminated as a nonradiative decay route.

An interesting method of increasing the rate of an observed cooling effect would be to increase the temperature from which the solution is cooled. In this study, the solution was always optically cooled from room temperature. If the initial temperature of the solution is higher, then, by the Boltzmann distribution, more molecules will populate higher vibrational levels of the ground S_0 state, and so more pump beam will be absorbed, inducing larger cooling efficiencies.

The obvious application for this laser-induced optical cooling mechanism is as a high-tech refrigerator, although the practicalities and economics of such a use would need refining. One such necessity could be the incorporation of the dye into a solid-state matrix, although presently no such host media exists. In polymers and silica gels,[33] laser dyes currently show low threshold to laser damage, and mechanisms for nonradiative decay routes that input thermal energy into the system are introduced.

Another foreseen application is in the components for optical computing. Many nonlinear optical materials based on molecules become warm and break down under irradiation by intense light. However if instead the material cools, there will be fewer "hot" molecules to absorb the laser energy and the rate of cooling will slow. In other words, the material will have an in-built thermostat and, importantly, will allow resonance nonlinearities to be exploited. The results of a preliminary investigation of the nonlinear optical properties of solution-phase rhodamine 101 using coherent anti-Stokes Raman scattering techniques are encouraging;[34] the end result could be stable, self-regulating materials for optical computing.

Acknowledgment. The authors would like to thank Professor D. Phillips for the provision of laser equipment. J.L.C. would like to acknowledge receipt of an EPSRC postgraduate studentship. We are also grateful for helpful comments from Dr. I. UlHaq and Dr. D. Clapton, from research instruments division of Oxford Instruments (U.K.).

Appendix

The rate of flow of heat between the sample and the surroundings is given by

$$C_V = \frac{\bar{\mathrm{d}}q}{\mathrm{d}T} \tag{A1}$$

where C_V is the constant volume heat capacity. Substituting in

eq A1 for the inexact differential $\bar{d}q$ with $P_{total}\,dt$ gives

$$dT = \frac{P_{total}\,dt}{C_V} \tag{A2}$$

where P_{total} is the total power given by the sum of the applied power, $P_{applied}$, and the radiative heat load, P_{load}, which is related to the difference in temperature between the sample, T_S, and the surrounding chamber, T_C, by

$$P_{load} = \sigma \frac{A_S}{\frac{1}{\epsilon_S} + \frac{A_S}{A_C}\left(\frac{1}{\epsilon_C} - 1\right)} ({T_C}^4 - {T_S}^4) \qquad \text{(watts)} \tag{A3}$$

where σ is Stefan's constant (5.7×10^{-8} W m^{-2} K^{-4}). ϵ_S and ϵ_C are emissivities of the sample and chamber, respectively. A_S and A_C are the areas of the sample and chamber surroundings, respectively.

For small temperature differences this can be approximated by

$$P_{load} = 4\sigma \frac{A_S}{\frac{1}{\epsilon_S} + \frac{A_S}{A_C}\left(\frac{1}{\epsilon_C} - 1\right)} {T_C}^3 (T_C - T_S) \qquad \text{(watts)} \tag{A4}$$

defining the characteristic rate constant, k, as

$$k = 4\sigma \frac{A_S}{\frac{1}{\epsilon_S} + \frac{A_S}{A_C}\left(\frac{1}{\epsilon_C - 1}\right)} \frac{{T_C}^3}{C_V} \qquad (s^{-1}) \tag{A5}$$

and substituting eq A4 into A2 gives

$$dT_S = \left(\frac{P_{applied} + P_{load}}{C_V}\right) dt = \left(\frac{P_{applied}}{C_V} + k(T_C - T_S)\right) dt \tag{A6}$$

The solution of this differential equation with the initial condition that at $t = 0$, $T_S = T_{S,t=0}$ gives

$$T_C - T_S = (T_C - T_{S,t=0}) \exp^{-kt} + \frac{P_{applied}}{kC_V}(\exp^{-kt} - 1) \qquad \text{(K)} \tag{A7}$$

If initially $T_C = T_{S,t=0}$, then the equation reduces to

$$T_C - T_S = \frac{P_{applied}}{kC_V}(\exp^{-kt} - 1) \qquad \text{(K)} \tag{A8}$$

Alternatively, if $T_C \neq T_S$ and the applied power is removed, eq A7 reduces to

$$T_C - T_S = (T_C - T_{S,t=0}) \exp^{-kt} \qquad \text{(K)} \tag{A9}$$

For small values of kt the exponents in eqs A8 and A9 can be simplified using a Taylor expansion. Taking only the first two terms in the expansion, eq A8 can be approximated by

$$T_C - T_S \cong \frac{-P_{applied}}{C_V} t \qquad \text{(K)} \tag{A10}$$

and equation A9 by

$$T_C - T_S \cong (T_C - T_{S,t=0})(1 - kt) \qquad \text{(K)} \tag{A11}$$

References and Notes

(1) Pringsheim, P. *J. Phys., USSR* **1946**, *10*, 495.
(2) Vavilov, S. *J. Phys., USSR* **1946**, *10*, 499.
(3) Landau, L. *J. Phys., USSR* **1946**, *10*, 503.
(4) Djeu, N.; Whitney, W. T. *Phys. Rev. Lett.* **1981**, *46*, 236.
(5) Tsujikawa, I.; Murao, T. *J. Phys. Soc. Jpn.* **1963**, *18*, 503.
(6) Kushida, T.; Geusic, J. E. *Phys. Rev. Lett.* **1968**, *21*, 1172.
(7) Epstein, R. I.; Buchwald, M, I.; Edwards, B. C.; Gosnell, T. R.; Mungan, C. E. *Nature* **1995**, *377*, 500.
(8) Mungan, C. E.; Buchwald, M. I.; Edwards, B. C.; Epstein, R. I.; Gosnell, T. R. *Phys. Rev. Lett.* **1997**, *78*, 1030.
(9) Zander, C.; Drexhage, K. H. In *Advances in Photochemistry*; Neckers, D. C., Volman, D. H., Von Bünau, G. Eds.; Wiley: New York, 1995; p 59.
(10) Clark, J. L.; Rumbles, G. *Phys. Rev. Lett.* **1996**, *76*, 2037.
(11) Mungan, C. E.; Gosnell, T. R. *Phys. Rev. Lett.* **1996**, *77*, 2840.
(12) Rumbles, G.; Clark, J. L. *Phys. Rev. Lett.* **1996**, *77*, 2841.
(13) Erikson, L. E. *J. Luminescence* **1972**, *5*, 1.
(14) Itagi, S. V.; Kulkarni, A. *Indian J. Pure Appl. Phys.* **1982**, *20*, 244.
(15) Blau, W.; Dankesreiter, W.; Penzkofer, A. *Chem. Phys. Lett.* **1984**, *85*, 473.
(16) Karstens, K.; Kobs, K. *J. Phys. Chem.* **1980**, *84*, 1871.
(17) Chang, M. S.; Elliott, S. S.; Gustafson, T. K.; Hu, C.; Jain, R. K. *IEEE, J. Quantum Electron.* **1972**, *8*, 527.
(18) Bloor, D.; Cross, G.; Sharma, P. K.; Elliott, J. A.; Rumbles, G. *J. Chem. Soc., Faraday Trans.* **1993**, *89*, 4013.
(19) Mukherjee, A. *Appl. Phys. Lett.* **1993**, *62*, 3423.
(20) Bradley, D. J.; Hutchinson, M. H. R.; Koetser, H.; Morrow, T.; New, G. H. C.; Petty, M. S. *Proc. R. Soc. London A* **1972**, *328*, 97.
(21) Gomes, A. S. L.; Boyer, G. R.; Demouchy, G.; Mysyrowicz, A.; Poignant, H.; Monerie, M. *Opt. Commun.* **1993**, *95*, 246.
(22) Chow, A.; Kennedy, J.; Pottier, R.; Truscott, T. G. *Photobiochem. Photobiophys.* **1986**, *11*, 139.
(23) Lu, Y.; Penzkofer, A. *Chem. Phys.* **1986**, *107*, 175.
(24) López Arbeloa, F.; Ruiz Ojeda, P.; López Arbeloa, I. *Chem. Phys. Lett.* **1988**, *148*, 253.
(25) Ruiz Ojeda, P.; Katime, I. A.; Ochoa, J. Ramón; López Arbeloa, I. *J. Chem. Soc., Faraday Trans. 2*, **1988**, *84*, 1.
(26) Lutz, H.; Luisi, P. L. *Helv. Chem. Acta* **1983**, *66*, 1929.
(27) Balshaw, N. H. *Practical Cryogenics: An Introduction to Laboratory Cryogenics*; Oxford Instruments: U.K., 1996; Vol. OI 151, p 68.
(28) Drexhage, K. H. *Topics in Applied Physics*; Springler-Verlag: Berlin, 1977; Vol 1, p 144.
(29) Dhami, S.; de Mello, A. J.; Rumbles, G.; Bishop, S. M.; Phillips, D; Beeby, A. *Photochem. Photobiol.* **1995**, *61*.
(30) Birks, J. B. *Photophysics of Aromatic Molecules*; Wiley: London, 1970.
(31) de Mello, A. J.; Ellott, J. A.; Rumbles, G. *J. Chem. Soc., Faraday Trans.* **1997**, *93*, 4723.
(32) Amat-Guerri, F.; Costella, A.; Floida, J. M.; Sastre, R. *Chem. Phys. Lett.* **1993**, *209*, 352.
(33) Lo, D.; Parris, J. E.; Lawless, J. L. *Appl. Phys. B* **1993**, *B56*, 385.
(34) Clark, J. L. Ph.D. Thesis, University of London, 1997.